
Article:
Anastopoulos Tzanis, M. S., Ham, C. J., Snyder, P. B. et al. (1 more author) (2020) Peeling-ballooning stability of tokamak plasmas with applied 3D magnetic fields. Nuclear Fusion. 106003. ISSN 1741-4326

https://doi.org/10.1088/1741-4326/aba451

Peeling-Ballooning Stability of Tokamak Plasmas With Applied 3D Magnetic Fields

M.S. Anastopoulos Tzanis [1,2], C.J. Ham [2], P.B. Snyder [3], H.R. Wilson [1,2]

1) York Plasma Institute, Department of Physics, University of York, York, YO10 5DD, UK
2) Culham Centre for Fusion Energy, Abingdon, Oxfordshire OX14 3DB, UK
3) General Atomics, San Diego, California 92186-5608, USA

31 July 2020

Abstract. The poloidal harmonics of the toroidal normal modes of an unstable axisymmetric tokamak plasma are employed as basis functions for the minimisation of the 3D energy functional. This approach presents a natural extension of the perturbative method considered in [M.S. Anastopoulos Tzanis *et al*, *Nuclear Fusion* **59**:126028, 2019]. This variational formulation is applied to the stability of tokamak plasmas subject to external non-axisymmetric magnetic fields. A comparison of the variational and perturbative methods shows that for D-shaped, high β_N plasmas, the coupling of normal modes becomes strong at experimentally relevant applied 3D fields, leading to violation of the assumptions that justify a perturbative analysis. The variational analysis employed here addresses strong coupling, minimising energy with respect to both toroidal and poloidal Fourier coefficients. In general, it is observed that ballooning unstable modes are further destabilised by the applied 3D fields and field-aligned localisation of the perturbation takes place, as local ballooning theory suggests. For D-shaped high β_N plasmas, relevant to experimental cases, it is observed that the existence of intermediate n unstable peeling-ballooning modes, where a maximum in the growth rate spectrum typically occurs, leads to a destabilising synergistic coupling that strongly degrades the stability of the 3D system.

1. Introduction

H-mode tokamak plasma operation, which has beneficial characteristics for fusion power performance and will be the baseline operational mode of the International Thermonuclear Experimental Reactor (ITER) [1], is intrinsically linked with the destabilisation of ideal magneto-hydrodynamic (MHD) instabilities, called the peeling-ballooning (PB) modes [2][3][4]. Those ideal MHD instabilities arise due to the establishment of steep pressure gradient and large current density in a narrow "pedestal" region at the edge of the core plasma. The PB modes are postulated to drive Edge Localised Modes (ELMs), which are field-aligned filamentary structures that erupt from the pedestal plasma, leading to large particle and heat transport. In large scale tokamak

devices like ITER, these transient phenomena, if uncontrolled, will exceed the melting point of the divertor tiles [5][6], shortening the life of the divertor.

One promising method to control ELMs applies non-axisymmetric magnetic perturbations (MPs) that lead to ELM mitigation [7][8][9][10], i.e. increase of ELM frequency and decrease of ELM energy loss, or complete ELM suppression [11][12][13][14], i.e. no ELMs. The key physics component that allows and defines the existence of those two operational states is still an active area of research. However, recent experimental and theoretical analysis, points towards a role for the degradation of the local and global stability of the tokamak plasma. In particular, the imposed 3D fields lead to local changes of plasma equilibrium parameters, that play a crucial role in determining the stability of the plasma. This leads to the destabilisation of high n ‡ ideal ballooning modes, where n is the toroidal mode number of the perturbation, which is localised about the most unstable magnetic field lines [15][16][17]. Such a feature is computationally and experimentally observed in ASDEX-Upgrade (AUG) discharges, when ELM mitigation occurs [18].

Additional numerical investigation of the PB stability of ELM mitigated discharges in AUG, showed that those discharges should be stable against global PB modes [19][20]. However, this analysis is based on stability codes for axisymmetric equilibria, where coupling of the toroidal normal modes is prohibited, i.e. the toroidal mode number remains a "good" quantum number. To improve our understanding it is important to consider the local and global stability of the 3D plasma equilibrium. An additional indication of the degradation of the global MHD stability boundary in such cases is related to experimental observations, where ELM suppression occurs below a pressure contour [14], of lower pressure compared to the stability boundary of the axisymmetric case. As such, the difference between ELM mitigation and suppression is postulated in Ref.[20] and Ref.[21] to be a competition between density pump-out that reduces the plasma pressure, i.e. global PB modes become more stable, and the degradation of the global ideal MHD stability boundary due to the presence of the 3D MPs.

The axisymmetric equilibrium geometry of the tokamak plasma provides a set of eigenmodes with discrete toroidal Fourier modes that can be studied individually. Therefore, the numerical complexity of the global plasma stability is reduced and is routinely and efficiently calculated with codes like ELITE [22] or MISHKA [23]. However, if a non-axisymmetric equilibrium is established, different Fourier harmonics of a particular toroidal mode number are coupled together satisfying the condition $n \pm n' = \lambda N$, where $n,\ n'$ are the toroidal mode numbers of the perturbation and N is the primary toroidal mode number of the non-axisymmetric equilibrium, with λ an integer. For a fixed n, a set of toroidal modes n' are coupled to form a "supermode" [24] of the n^{th} family. This feature significantly increases the numerical complexity for the stability of the system. This is especially true for edge localised perturbations, where large poloidal

‡ We will typically refer to low $n \sim 1-5$ which are global modes spanning the full minor radius, intermediate $n \sim 5-20$ which are radially localised and tap into the kink drive, and high n which are highly localised pressure driven ballooning modes with negligible kink drive.

and toroidal mode numbers must be considered, and then this feature significantly limits the radial resolution. As a result, the examination of unstable intermediate to high n perturbations that drive the onset of ELMs becomes truly challenging in non-axisymmetric geometry.

In order to minimise the numerical complexity of the non-axisymmetric system, a perturbation theory was introduced [25][26][27], considering an applied 3D magnetic field, B_N, which is several orders of magnitude lower than the confining axisymmetric magnetic field B_0; typically $B_N/B_0 \sim 10^{-5} - 10^{-3}$. The perturbative approach assumes weak coupling, restricting consideration to $\lambda = [0, \pm 1]$, and leading to the formation of triplets of toroidal Fourier harmonics $\{n - N, n, n + N\}$. To leading order the spatial structure of the three toroidal normal modes that couple is provided by the axisymmetric system. Such a perturbative approach requires weak coupling of toroidal normal modes, which is observed to be violated for strongly shaped, high β_N plasmas. In addition, the perturbative method does not allow freedom for the 3D field to adjust the relative size of the poloidal harmonics that couple to form each toroidal normal mode of the axisymmetric system. The above restrictions can be overcome by considering a variational formulation of the non-axisymmetric energy functional that uses the poloidal Fourier harmonics of the toroidal normal modes of the axisymmetric system as basis functions. The energy can be minimised with respect to the poloidal coupling coefficients that are introduced to vary the relative amplitude of these poloidal and toroidal harmonics.

Such an approach can be physically motivated as follows. In an axisymmetric tokamak plasma, intermediate to high toroidal mode number, n, peeling-ballooning modes involve a single toroidal Fourier harmonic, but couple a number of poloidal Fourier harmonics. For the ballooning component, each poloidal harmonic, m, has the same shape, and each is centred on its corresponding rational surface where $m = nq$ (q being the safety factor). The relative amplitude of these Fourier modes is determined by to the radial variation of the equilibrium. With the application of a 3D MP there is an additional coupling of the toroidal Fourier harmonics and, in addition, this can influence the relative amplitude of the poloidal Fourier harmonics. However, the radial shape of each poloidal harmonic is not expected to be modified by the applied MP. Guided by this physics understanding, we employ a new variational approach where the trial function is the set of axisymmetric poloidal Fourier harmonics (each with a radial dependence corresponding to that for the axisymmetric plasma) and treat the coefficients that scale each as a set of variational parameters, obtained by minimising the energy functional.

The paper is set as follows. Section 2 presents our new variational formulation of the non-axisymmetric energy functional, which is composed of an axisymmetric and non-axisymmetric component, that leads to a generalised eigenvalue problem to be solved numerically. Section 3 presents results from the application of this technique to applied MPs for different plasma β_N and cross-section shapes, in an attempt to understand the underlying difference between the stability of an axisymmetric and non-

axisymmetric system. Finally, Section 4 discusses the obtained results and their relation to experimental observations.

2. Variational 3D MHD Stability

In this section, the non-axisymmetric tokamak plasma stability theory is described using a new variational approach. The general numerical framework for a perturbative approach, i.e. calculation of non-axisymmetric plasma response and stability, based on the axisymmetric stability code ELITE, was presented in Ref.[27]. Here, we extend that formalism to develop a new variational approach to stability that is valid for a wide range of 3D magnetic fields. ELITE provides a particularly efficient and accurate approach to calculate the radial dependence of each axisymmetric Fourier mode, providing our set of basis functions for the variational method.

The ideal MHD stability of tokamak plasmas under the application of external non-axisymmetric MPs of single toroidal mode number N is considered. The stability problem results in a generalised eigenvalue problem of the force operator $\boldsymbol{F}$ and the stability of the system will depend on the eigenvalues of this operator. The variational approach employs a set of orthogonal basis functions for the representation of a non-zero plasma displacement $\boldsymbol{\delta\xi} \neq 0$ and provides a method that determines an appropriate superposition of these basis functions that minimises the potential δW and kinetic δK energy change of the non-axisymmetric equilibrium state. This provides the most unstable mode that can be produced from the particular basis set. Considering that the applied 3D fields are much smaller than the axisymmetric equilibrium fields, the poloidal Fourier coefficients derived from the axisymmetric equilibrium are adopted as appropriate trial functions for energy minimisation. The radial dependence of the poloidal Fourier harmonics is taken to be the same as for the axisymmetric system, each weighted by a "coupling coefficient" to adjust their relative size. Coupling of different toroidal Fourier harmonics is also accommodated in our approach. The minimisation of the energy functional determines the coupling coefficients.

2.1. Potential and Kinetic Energy Terms

The coordinate system is based on the axisymmetric normal $\hat{\boldsymbol{n}} = \nabla\psi_0/|\nabla\psi_0|$, binormal $\hat{\boldsymbol{t}} = (\boldsymbol{B}_0 \times \nabla\psi_0)/(B_0|\nabla\psi_0|)$ and parallel $\hat{\boldsymbol{b}} = \boldsymbol{B}_0/B_0$ components. Here ψ_0 labels the flux surfaces and $\boldsymbol{B}_0$ is the magnetic field of the axisymmetric equilibrium, i.e. before application of the 3D MP. The parallel component of the displacement $\boldsymbol{\delta\xi}_\parallel$ contributes only to the kinetic energy δK and fluid compression $\nabla \cdot \boldsymbol{\delta\xi}$. Therefore, at marginal stability minimisation of the potential energy δW with respect to $\boldsymbol{\delta\xi}_\parallel$ requires $\nabla\cdot\boldsymbol{\delta\xi} = 0$. For most magnetic configurations, the minimisation of fluid compression is achieved by setting an appropriate form for the parallel displacement $\boldsymbol{\delta\xi}_\parallel$ [28]. This is the so-called incompressible limit, and neglects the contribution of $\delta\xi_\parallel$ to inertia, leading to an overestimate for the growth rate. Although, its contribution can in principle be

accounted for by scaling the growth rate by $1/\sqrt{1+2q^2}$ [29]. We shall adopt this incompressible model, and as such, only the perpendicular dynamics are considered. The displacement is then reduced to the two components perpendicular to $\hat{\boldsymbol{b}}$, which we denote X and U,

$$\boldsymbol{\delta\xi} \rightarrow \boldsymbol{\delta\xi}_{\perp} = \frac{X}{|\nabla\psi_0|}\hat{\boldsymbol{n}} + U\frac{|\nabla\psi_0|}{B_0}\hat{\boldsymbol{t}} \tag{1a}$$

Minimisation of the axisymmetric magnetic compression, relates the two components,

$$[\frac{f}{B_0^2}(\boldsymbol{B}_0\cdot\nabla) - \partial_\phi]U = [\partial_\psi + \partial_\psi(\ln \mathcal{J}_0 B_0^2) + \frac{2\mu_0\partial_\psi p_0}{B_0^2}]X \tag{1b}$$

where $f(\psi) = RB_{0t}$, B_{0t} is the toroidal magnetic field, $\mathcal{J}_0$ is the Jacobian of the orthogonal coordinate system and p_0 is the plasma pressure. Therefore, the displacement $\boldsymbol{\delta\xi}$ becomes a function of X.

Considering an ideal and incompressible limit for the stability, a displacement $\boldsymbol{\delta\xi}$ (i.e. the peeling-ballooning mode) of the plasma equilibrium (i.e. axisymmetric + non-axisymmetric) will result in a force,

$$\boldsymbol{F} = \boldsymbol{J}\times\boldsymbol{\delta B} + \boldsymbol{\delta J}\times\boldsymbol{B} + \nabla(\boldsymbol{\delta\xi}\cdot\nabla p) \tag{2}$$

where ($\boldsymbol{\delta\xi}$, $\boldsymbol{\delta B}$, $\boldsymbol{\delta J}$) represent the perturbed displacement, magnetic field and current density associated with the instability. In order to express $\boldsymbol{F}$ in an ordered way, the plasma equilibrium can be split into an axisymmetric and non-axisymmetric part, i.e. $\boldsymbol{B} = \boldsymbol{B}_0 + \boldsymbol{B}_N$, $\boldsymbol{J} = \boldsymbol{J}_0 + \boldsymbol{J}_N$ and $p = p_0 + p_N$. The perturbed quantities, that arise from the displacement $\boldsymbol{\delta\xi}$, are linear with respect to equilibrium quantities and similarly,

$$\boldsymbol{\delta B} = \boldsymbol{\delta B}_n + \sum_{\pm}\boldsymbol{\delta B}_{n\pm N} \tag{3a}$$

$$\boldsymbol{\delta J} = \boldsymbol{\delta J}_n + \sum_{\pm}\boldsymbol{\delta J}_{n\pm N} \tag{3b}$$

$$\delta p = \delta p_n + \sum_{\pm}\delta p_{n\pm N} \tag{3c}$$

where the subscript indicates the toroidal mode number of the perturbation.

Substituting Eqn.(3) into the linearised force naturally results in ordered axisymmetric and non-axisymmetric contributions. Specifically, writing $\boldsymbol{F} = \boldsymbol{F}_0 + \boldsymbol{F}_1 + \boldsymbol{F}_2$, we have:

$$\boldsymbol{F}_0 = \boldsymbol{J}_0\times\boldsymbol{\delta B}_n + \boldsymbol{\delta J}_n\times\boldsymbol{B}_0 + \nabla(\boldsymbol{\delta\xi}_n\cdot\nabla p_0) \tag{4}$$

$$\boldsymbol{F}_1 = \sum_{\pm}[\boldsymbol{J}_0\times\boldsymbol{\delta B}_{n\pm N} + \boldsymbol{J}_{\pm N}\times\boldsymbol{\delta B}_n + \boldsymbol{\delta J}_n\times\boldsymbol{B}_{\pm N} + \boldsymbol{\delta J}_{n\pm N}\times\boldsymbol{B}_0 + \nabla(\boldsymbol{\delta\xi}_n\cdot\nabla p_{\pm N})] \tag{5}$$

$$\boldsymbol{F}_2 = \sum_{\pm}\boldsymbol{J}_{\pm N}\times\boldsymbol{\delta B}_{n\pm N} + \boldsymbol{\delta J}_{n\pm N}\times\boldsymbol{B}_{\pm N} \tag{6}$$

where $\boldsymbol{\delta B}_n = \nabla\times(\boldsymbol{\delta\xi}_n\times\boldsymbol{B}_0)$ and $\boldsymbol{\delta B}_{n\pm N} = \nabla\times(\boldsymbol{\delta\xi}_n\times\boldsymbol{B}_{\pm N})$. The zeroth order force, $\boldsymbol{F}_0$, is due to the original axisymmetric equilibrium and the first order, $\boldsymbol{F}_1$, arises due

to the non-axisymmetric equilibrium that provides the coupling between the toroidal axisymmetric modes. The second order force, $\boldsymbol{F}_2$, is dropped from the calculation, as it is assumed that $\boldsymbol{F}_2 \ll \boldsymbol{F}_1$. This is justified by the fact that $\boldsymbol{F}_2 \propto (B_N/B_0)^2$, while $\boldsymbol{F}_1 \propto (B_N/B_0)$ and $B_N \ll B_0$. Considering Eqn.(5) and taking the inner product with the complex conjugate perturbed displacement $\boldsymbol{\delta\xi}_n^*$, after some algebraic manipulation, we derive the following contribution to the perturbed energy. The kinetic energy,

$$\delta K(\boldsymbol{\delta\xi}_n^*, \boldsymbol{\delta\xi}_n) = \frac{1}{2}\int \boldsymbol{\delta\xi}_n^* \cdot \boldsymbol{\delta\xi}_n \; \mathcal{J}_0 \mathrm{d}\psi \mathrm{d}\theta^* \mathrm{d}\phi \tag{7}$$

the part of the potential energy associated with perturbations about the axisymmetric part of the equilibrium,

$$\begin{aligned}\delta W(\boldsymbol{\delta\xi}_n^*, \boldsymbol{\delta\xi}_n) = \frac{1}{2}\int \{ |\boldsymbol{\delta B}_{n\perp}|^2 - \frac{\boldsymbol{J_0 \cdot B_0}}{B^2}(\boldsymbol{\delta\xi}_{n\perp}^* \times \boldsymbol{B}_0)\cdot \boldsymbol{\delta B}_{n\perp} \\ - 2(\boldsymbol{\delta\xi}_{n\perp}\cdot\nabla p_0)(\boldsymbol{\delta\xi}_{n\perp}^*\cdot\boldsymbol{\kappa}_0)\} \; \mathcal{J}_0 \mathrm{d}\psi \mathrm{d}\theta^* \mathrm{d}\phi\end{aligned} \tag{8}$$

the part of the potential energy associated with perturbations about the 3D part of the equilibrium,

$$\begin{aligned}\delta Y(\boldsymbol{\delta\xi}_n^*, \boldsymbol{\delta\xi}_{n'}) = -\frac{1}{2}\int \{ [\boldsymbol{\delta\xi}_n^* \cdot (\boldsymbol{J}_N \times \boldsymbol{\delta B}_{n'} + \boldsymbol{\delta J}_{n'} \times \boldsymbol{B}_N)] \\ + [\nabla \times (\boldsymbol{\delta\xi}_n^* \times \boldsymbol{J}_0)] \cdot (\boldsymbol{\delta\xi}_{n'} \times \boldsymbol{B}_N) \\ - \boldsymbol{\delta J}_n^* \cdot (\boldsymbol{\delta\xi}_{n'} \times \boldsymbol{B}_N)\} \; \mathcal{J}_0 \mathrm{d}\psi \mathrm{d}\theta^* \mathrm{d}\phi\end{aligned} \tag{9}$$

and a surface contribution due to the 3D part of the equilibrium,

$$\begin{aligned}\delta S(\boldsymbol{\delta\xi}_n^*, \boldsymbol{\delta\xi}_{n'}) = -\frac{1}{2}\int \{ (\boldsymbol{\delta\xi}_n^* \cdot \boldsymbol{n})[(\boldsymbol{\delta\xi}_{n'} \times \boldsymbol{B}_N)\cdot \boldsymbol{J}_0 - \boldsymbol{\delta B}_{n'\pm N}\cdot \boldsymbol{B}_0] \\ + \boldsymbol{\delta B}_n^* \cdot [\boldsymbol{B}_N(\boldsymbol{\delta\xi}_{n'}\cdot\boldsymbol{n}) - \boldsymbol{\delta\xi}_{n'}(\boldsymbol{B}_N\cdot\boldsymbol{n})] \\ + (\boldsymbol{\delta\xi}_n^*\cdot\boldsymbol{n})(\boldsymbol{\delta\xi}_{n'}\cdot\nabla p_N)\} \; \mathcal{J}_0 \mathrm{d}\theta^* \mathrm{d}\phi\end{aligned} \tag{10}$$

where $n \neq n'$ are the toroidal mode numbers of the displacement $\boldsymbol{\delta\xi}$ and θ^* is straight field-line poloidal angle.

2.2. Variational Formulation of Energy Functional

The ideal MHD system defines a Hermitian stability problem, so that $\delta W_{n,n'} = \delta W_{n',n}$, where $\delta W_{n,n'} = \delta W(\boldsymbol{\delta\xi}_n^*, \boldsymbol{\delta\xi}_{n'})$. Thus, it can efficiently be solved by expanding in a set of discrete normal modes. Considering the stability of the axisymmetric system and non-degenerate eigenvalues $\omega_{n'}^2 \neq \omega_n^2$ for $n' \neq n$,

$$(\omega_{n'}^2 - \omega_n^2)(\delta K_{n',n} - \delta K_{n,n'}) = (\delta W_{n',n} - \delta W_{n,n'}) = 0 \tag{11}$$

and leads to $\delta K_{n,n'} = \delta_{n,n'}$, where $\delta K_{n,n'} = \delta K(\boldsymbol{\delta\xi}_n^*, \boldsymbol{\delta\xi}_{n'})$. As a result, the axisymmetric normal modes $\boldsymbol{\delta\xi}_n^{(0)}$ are orthogonal and can be used to define a basis set, through which

any perturbation can be expressed as a superposition of these modes. Let us now define $\boldsymbol{\delta\xi}_n^{(0)}$ to be the displacement eigenfunction associated with the axisymmetric system. This displacement $\boldsymbol{\delta\xi}_n^{(0)}$ can be expressed as a sum of terms each linear in the radial displacement $X_n(\psi,\theta^*)$ [28]. Expanding in poloidal Fourier modes, $X_n(\psi,\theta^*) = \sum_m X_{n,m}(\psi)\exp[-im\theta^*]$, where the radially dependent function $X_{n,m}(\psi)$ can be provided by ELITE. Note that for any constant d_n, $\boldsymbol{\delta\xi}(d_nX_n) = d_n\boldsymbol{\delta\xi}(X_n)$. Furthermore, the linearised force is linear with respect to the displacement, and therefore X_n; thus $\boldsymbol{F}(d_nX_n) = d_n\boldsymbol{F}(X_n)$ and similarly $\delta W(d^*_{n'}X^*_{n'}, d_nX_n) = d^*_{n'}d_n\delta W(X^*_{n'}, X_n)$. The same applies to δK, δY and δS.

In order to create orthogonal normal modes, the toroidal dependence of the displacement is expressed through Fourier harmonics. As such, a displacement can be expressed as a linear superposition of axisymmetric normal modes $\boldsymbol{\delta\xi}_n$,

$$\boldsymbol{\delta\xi}_n(\psi,\theta^*,\phi) = \sum_{n'} d_{n'}\boldsymbol{\delta\xi}^{(0)}_{n'}(\psi,\theta^*)e^{in'\phi} = \sum_{n'} d_{n'}\boldsymbol{\delta\xi}^{(0)}_{n'}(X_{n'})e^{in'\phi} \tag{12}$$

In the case where the plasma equilibrium is axisymmetric, the energy functional results in a toroidally decoupled system and $d_{n'} = \delta_{n,n'}$ for a specific n. This simplifies the problem and allows the ψ-dependence and relative size of all Fourier coefficients $X_{n,m}(\psi)$ (see above) to be calculated in a code like ELITE. If non-axisymmetric fields are present, toroidal modes become coupled through the non-axisymmetric potential energy δY and δS and the resulting energy principle becomes,

$$\begin{aligned}\sum_n |d_n|^2\omega_n^2\delta K_{n,n} = &\sum_n |d_n|^2\delta W_{n,n} \\ &+ \sum_{n,n'} d^*_n d_{n'}\delta Y_{n,n'}\delta_{n,n'\pm N} \\ &+ \sum_{n,n'} d^*_n d_{n'}\delta S_{n,n'}\delta_{n,n'\pm N}\end{aligned} \tag{13}$$

where $\delta Y_{n,n'} = \delta Y(\boldsymbol{\delta\xi}^*_n, \boldsymbol{\delta\xi}_{n'})$, $\delta S_{n,n'} = \delta S(\boldsymbol{\delta\xi}^*_n, \boldsymbol{\delta\xi}_{n'})$ and N is the toroidal mode number associated with 3D equilibrium quantities in the energy terms. This approach will later be referred to as "Variational Toroidal Mode Coupling".

If the $\delta Y_{n,n'}$ and $\delta S_{n,n'}$ coefficients are small, weak coupling occurs and it is expected that the above variational method is equivalent to the perturbative method presented in Ref.[27]. An advantage of the variational method is that it is not restricted to weak coupling as larger values of $\delta Y_{n,n'}$ and $\delta S_{n,n'}$ can accommodate strong or broadband coupling of toroidal modes. However, in both approaches the trial function forces the mix of poloidal Fourier harmonics to equal that of the axisymmetric normal modes $\boldsymbol{\delta\xi}^{(0)}_n(\psi,\theta^*,\phi)$. As a result, any influence of the applied 3D field on the coupling of the individual poloidal harmonics cannot be captured by this approach and the structure of the non-axisymmetric normal mode is likely overly constrained.

In order to resolve this issue, we adopt a trial function that expands in both poloidal

and toroidal Fourier harmonics of the axisymmetric system $\boldsymbol{\delta\xi}^{(0)}_{n,m}(\psi)$,

$$\boldsymbol{\delta\xi}_n(\psi,\theta^*,\phi) = \sum_{n',m'} c_{n',m'}\boldsymbol{\delta\xi}^{(0)}_{n',m'}(\psi)e^{-(im'\theta^*-n'\phi)} = \sum_{n',m'} c_{n',m'}\boldsymbol{\delta\xi}^{(0)}_{n',m'}(X_{n',m'})e^{-i(m'\theta^*-n'\phi)} \tag{14}$$

where $X_{n',m'}(\psi)$ are the Fourier coefficients derived from the axisymmetric system. For the axisymmetric system, such a representation results in a system of normal modes, where each has a single toroidal Fourier mode, but is a superposition of many poloidal Fourier modes due to poloidal inhomogeneity of the axisymmetric equilibrium. Thus, for the axisymmetric system $c_{n',m'} = 1$. It is straight forward to derive an energy principle for the non-axisymmetric system, which becomes

$$\begin{aligned}\sum_{n,m,m',m''} c^*_{n,m}c_{n,m'}\omega^2_n\delta K^{m,m'}_{n,n}\delta^{m,m'+m''} = &\sum_{n,m,m',m''} c^*_{n,m}c_{n,m'}\delta W^{m,m'}_{n,n}\delta^{m,m'+m''} \\ &+ \sum_{n,n',m,m',m''} c^*_{n,m}c_{n',m'}\delta Y^{m,m'}_{n,n'}\delta^{m,m'+m''}_{n,n'\pm N} \\ &+ \sum_{n,n',m,m',m''} c^*_{n,m}c_{n',m'}\delta S^{m,m'}_{n,n'}\delta^{m,m'+m''}_{n,n'\pm N}\end{aligned} \tag{15}$$

where $\delta K^{m,m'}_{n,n} = \delta K(\boldsymbol{\delta\xi}^{(0)}_{n,m}, \boldsymbol{\delta\xi}^{(0)}_{n,m'})$, $\delta W^{m,m''}_{n,n} = \delta W(\boldsymbol{\delta\xi}^{(0)}_{n,m}, \boldsymbol{\delta\xi}^{(0)}_{n,m'})$, $\delta Y^{m,m'}_{n,n'} = \delta Y(\boldsymbol{\delta\xi}^{(0)}_{n,m}, \boldsymbol{\delta\xi}^{(0)}_{n',m'})$, $\delta S^{m,m'}_{n,n'} = \delta S(\boldsymbol{\delta\xi}^{(0)}_{n,m}, \boldsymbol{\delta\xi}^{(0)}_{n',m'})$, m'' is the poloidal mode number and N the toroidal mode number associated with equilibrium quantities in the energy terms. Taking the coefficients $c_{n',m'}$ as variational parameters, and minimising the energy with respect to $c^*_{n,m}$, provides a set of equations for the numerical coefficient $c_{n',m'}$. These equations depend on the matrix elements $\delta K^{m,m'}_{n,n}$, $\delta W^{m,m'}_{n,n}$, $\delta Y^{m,m'}_{n,n'}$ and $\delta S^{m,m'}_{n,n'}$, which can all be derived from axisymmetric ELITE calculations for a given toroidal mode number (n or $n \pm N$). This approach will later be referred to as "Variational Poloidal & Toroidal Mode Coupling".

It can be observed from Eqn.(15) that this minimisation will adjust the coupling of poloidal harmonics for each toroidal normal mode and this can be significant when strong coupling occurs providing greater flexibility in the trial function to optimise the poloidal mode structure. In this case, the structure of each toroidal normal mode in the presence of a 3D MP can differ significantly from the axisymmetric modes. In principle, such a feature can allow the 3D MP to adjust the coupling between external kink/peeling modes and core ballooning modes, as the corresponding poloidal harmonics can change independently. In addition, in a tokamak plasma, elongation and triangularity lead to coupling of $\{m, m \pm 1, m \pm 2\}$ poloidal modes, whereas in a non-axisymmetric plasma additional shaping effects can significantly increase the number of coupled poloidal harmonics, indicating the importance of allowing freedom in their coupling. Together with our physics understanding of ballooning modes in an axisymmetric plasma, i.e. that the $X_{n,m}(\psi)$ are all very similar for a given n for all m, only the relative coupling adjusts; this gives us confidence that our trial function will accurately capture the effect of MPs on the PB stability.

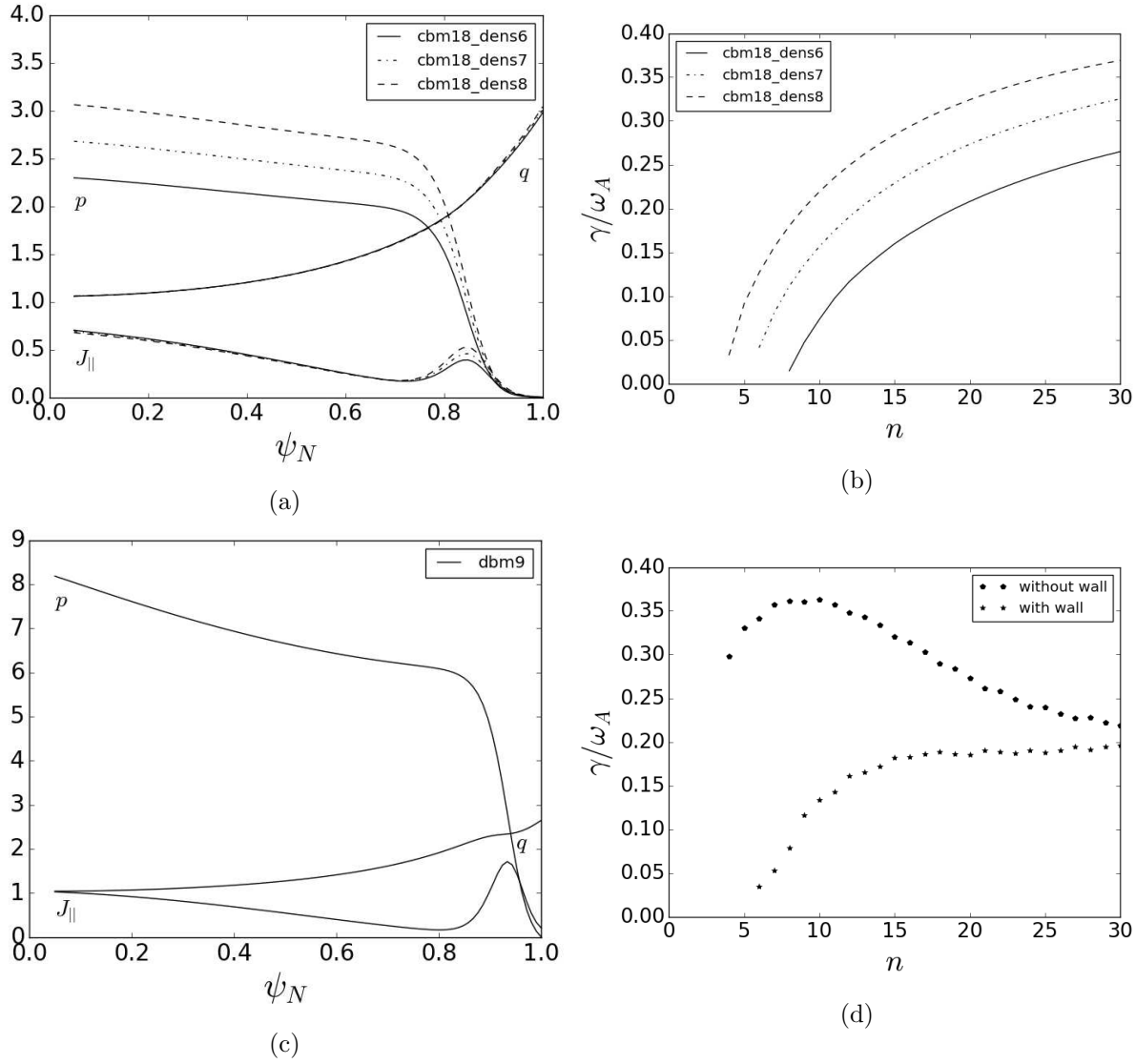

Figure 1: The flux dependence of the equilibrium pressure p [$10 \cdot$ kPa] and parallel current density $J_{||}$ [MAm^{-2}] as well as the q-profile for the (a) circular (*cbm*18) and (c) D-shaped (*dbm*9) equilibria. The growth rate spectrum of the unstable peeling-ballooning modes as a function of toroidal mode number n for the (b) circular (*cbm*18) and (d) D-shaped (*dbm*9) axisymmetric equilibria.

3. Application to External MPs

3.1. Linear Plasma Response to Applied MPs

The ELITE code has been extended, and used at marginal stability to obtain the linear, ideal MHD plasma response for a given non-axisymmetric magnetic flux perturbation of toroidal mode number, N, at the plasma-vacuum interface, as described in Ref.[27]. Due to the low N applied field the low-n version of ELITE [30] is used. Two plasma shapes are considered, one for a large aspect ratio circular plasma cross-section based on the

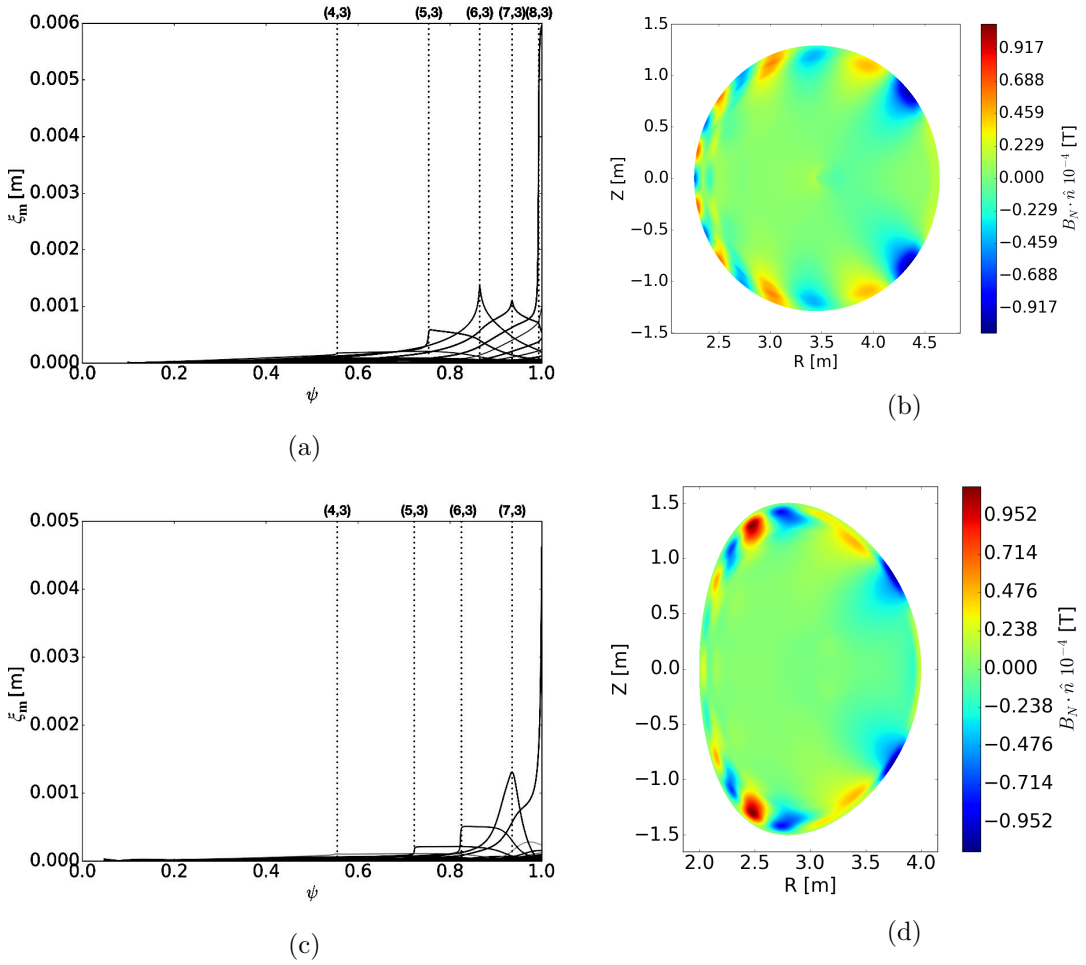

Figure 2: Linear, ideal MHD plasma response to an applied $N = 3$ even MP. The radial dependence of the straight field line poloidal harmonics of the normal displacement functional $\boldsymbol{\xi}_N \cdot \nabla\psi$ [m] for the (a) circular (*cbm*18_*dens*6) and (c) D-shaped (*dbm*9) equilibrium. The reconstruction in the poloidal cross-section of the normal magnetic field $\boldsymbol{B}_N \cdot \hat{\boldsymbol{n}}$ [T] for the (b) circular (*cbm*18_*dens*6) and (d) D-shaped (*dbm*9) equilibrium.

circular cross-section (*cbm*18) equilibrium configurations and a second for a D-shaped (*dbm*9) equilibrium configuration created using the TOQ fixed boundary equilibrium code [31]. In both cases, an even $N = 3$ MP field is applied.

Considering first the circular (*cbm*18_*dens*6, *cbm*18_*dens*7 and *cbm*18_*dens*8) equilibrium configurations, the inverse aspect ratio $\epsilon = 0.3$, $\beta_N = [1.06, 1.31, 1.54]$ and $q_a = [2.97, 3.01, 3.04]$ respectively. Those axisymmetric plasma equilibria are ballooning unstable for $n > [7, 5, 3]$ for the three cases respectively. For the D-shaped (*dbm*9) equilibrium configuration, the inverse aspect ratio is $\epsilon = 0.3$, $\beta_N = 2.83$ and $q_a = 2.65$. This axisymmetric plasma equilibrium is unstable to low to intermediate n kink-ballooning modes, while the standard ballooning modes occur for high $n > 30 - 40$. In addition, to examine the impact of the applied MP on shaped high β_N plasmas where

the kink modes are suppressed (due to shaping or a conducting wall), for the D-shaped (*dbm*9) equilibrium an ideal conducting wall is introduced close to the plasma surface. The ideal wall is introduced by coupling ELITE with the VACUUM code [32]. The ideal wall has the same shape as the plasma boundary at a distance $(a_w - a)/a = 2\%$, where a_w and a are the wall and plasma minor radius respectively.

The axisymmetric equilibrium profiles of the circular (*cbm*18) and D-shaped (*dbm*9) cases, as well as the associated growth rate spectrum of the unstable peeling-ballooning modes, are shown in Fig.1. The linear plasma response for an even (up/down symmetric) $N = 3$ MP field is shown in Fig.2. Both responses are characterised by an external kink/peeling response.

3.2. Comparison of Perturbative and Variational Toroidal Mode Coupling

In this section we employ the variational approach which fixes the poloidal spectrum (equal to the axisymmetric spectrum), and use variational theory to determine the coupling of different n ballooning modes. The matrix elements $F_{nn'}$ for the perturbative approach described in Ref.[27] and the variational approach described in this work, come from a similar set of equations and the only difference occurs in normalisation of the individual basis set. A straightforward relation exists between the two methods, if the relative poloidal coupling of the axisymmetric normal modes remains unchanged for a given n, such that

$$F^{(1)}_{nn'} = \frac{\delta Y_{n,n'\pm N} + \delta S_{n,n'\pm N}}{\sqrt{\delta K_{n,n} \delta K_{n',n'}}} \tag{16}$$

As a result, a direct comparison of the two approaches becomes possible. In addition, we can define a quantity, called the coupling coefficient $V_{nn'} = ||d_n|| = ||F^{(1)}_{nn'}/(\omega^2_{0n} - \omega^2_{0n'})||$, that measures the contribution of sideband harmonics $n \pm N$ to the displacement.

3.2.1. Circular cbm18 Case Initially the circular *cbm*18_*dens*6 equilibrium with the lowest $\beta_N = 1.06$ is considered, and only nearest neighbour coupling is taken into account, i.e. coupling of n with $n \pm N$. For applied field strength $B_N/B_0 < 10^{-3}$, where weak coupling occurs, the "variational toroidal coupling" method results in the same outcome as the perturbative method. Fig.3c illustrates a comparison for the growth rate between the two approaches considering a triplet mode with primary toroidal mode number $n = 21$. As can be observed up to $B_N/B_0 \sim 10^{-3}$ the two approaches agree very well, but as the field strength is increased a disagreement starts to build up and the two approaches diverge. The growth rate of the triplet in the variational case is observed to increase slower with the applied field since the coupling to the destabilising lower n modes becomes weaker in this case. In addition, in the perturbative analysis, the assumption of weak toroidal coupling means that the coupling coefficient of the primary mode n is unity, i.e. $||d_n|| = 1$. In the variational approach this assumption is relaxed and $||d_n|| \neq 1$, such that the perturbative method results in unphysical behaviour as B_N/B_0 increases.

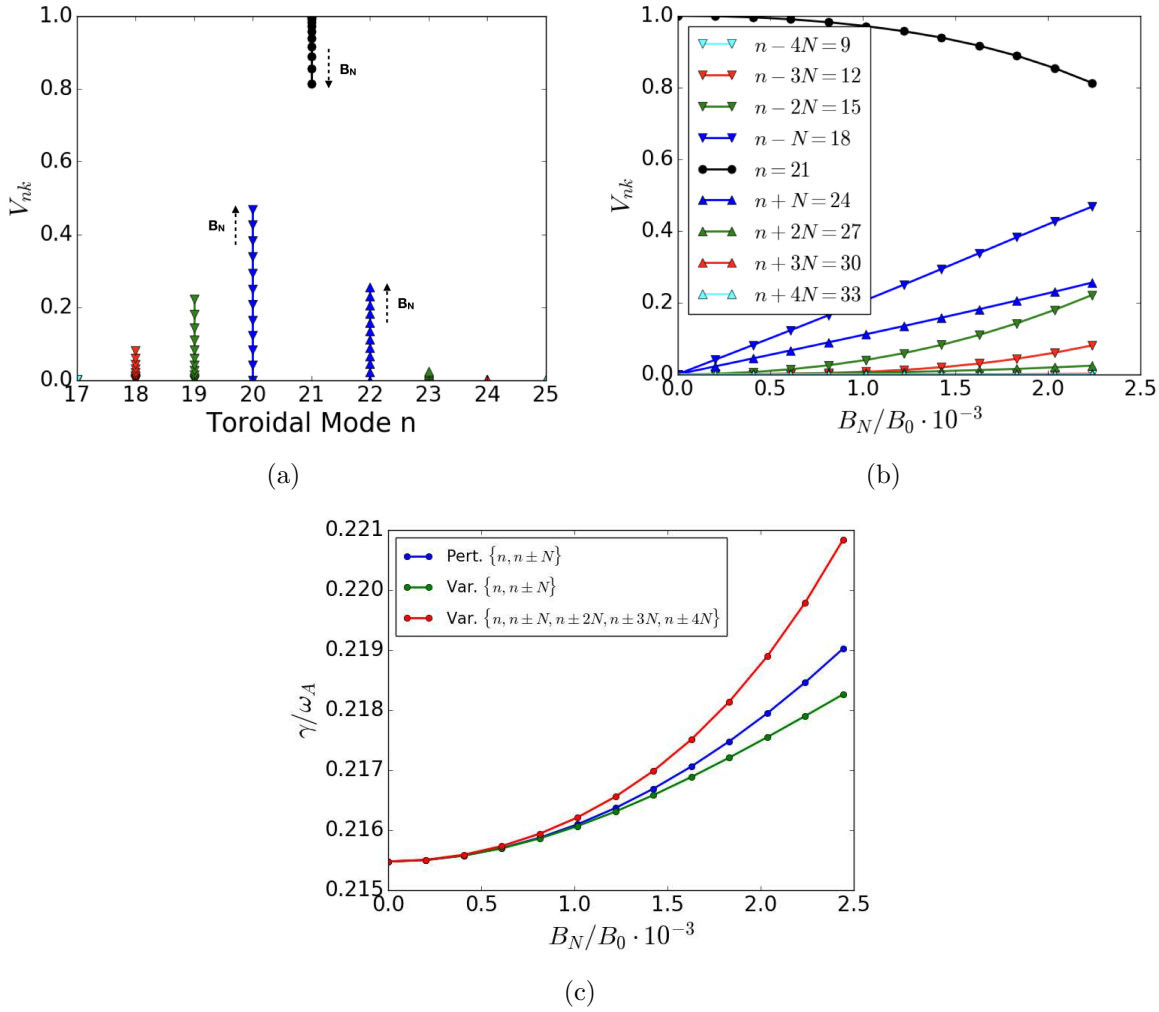

Figure 3: The coupling coefficients of a primary $n = 21$ mode for the circular *cbm*18_*dens*6 equilibrium of a nonuplet $\{n, n \pm N, n \pm 2N, n \pm 3N, n \pm 4N\}$ mode, (a) as a function of the toroidal mode number and (b) applied field strength B_N/B_0 using the "variational toroidal coupling" method. (c) Illustrates a comparison between the perturbative and "variational toroidal coupling" methods for a triplet $\{n, n \pm N\}$ and nonuplet $\{n, n \pm N, n \pm 2N, n \pm 3N, n \pm 4N\}$ mode.

Furthermore, the variational method allows the coupling of multiple toroidal normal modes. Since perturbation theory deviates at $B_N/B_0 \sim 10^{-3}$, it is expected that strong coupling occurs requiring more toroidal normal modes to be retained. As can be observed from Fig.3, with increasing applied field, multi-mode coupling takes place and in this case for $B_N/B_0 \sim 2.25 \cdot 10^{-3}$ even 3^{rd} neighbouring coupling is required, and further destabilisation is observed due to the inclusion of additional degrees of freedom. The $n = 21$ mode couples strongly to lower n neighbours, as indicated from the perturbative method considering only first neighbour coupling, with the 3^{rd} neighbour contributing $\sim 10\%$. In addition, the stronger coupling to lower n modes leads to

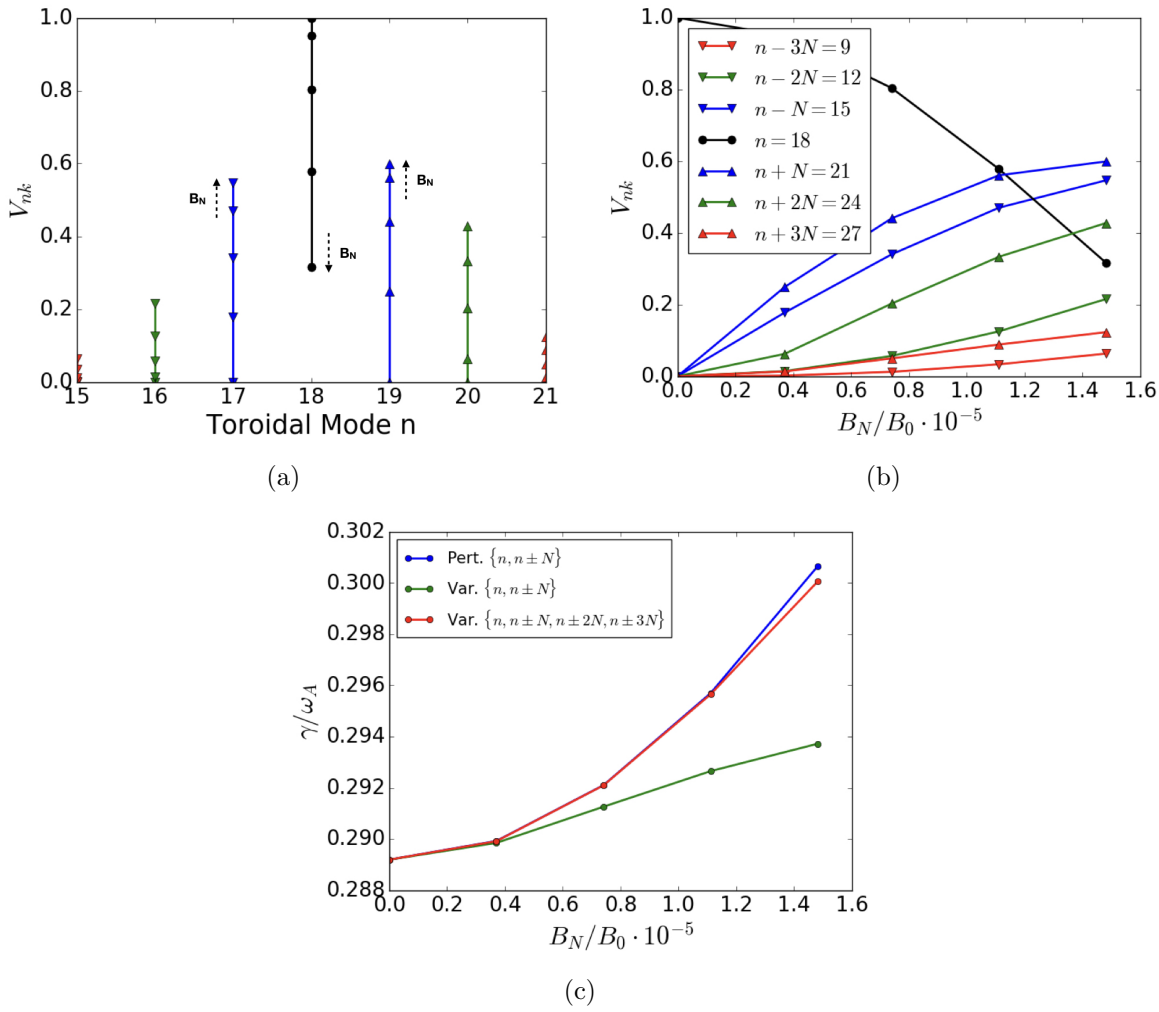

Figure 4: The coupling coefficients of a primary $n = 18$ mode for the D-shaped *dbm*9 equilibrium of a septuplet $\{n, n \pm N, n \pm 2N, n \pm 3N\}$ mode, (a) as a function of the toroidal mode number and (b) applied field strength B_N/B_0 using the variational method. (c) Illustrates a comparison between the perturbative and variational methods for a triplet $\{n, n \pm N\}$ and septuplet $\{n, n \pm N, n \pm 2N, n \pm 3N\}$ mode.

further destabilisation, as can be observed from Fig.3. In addition, it can be observed that with increasing field strength B_N/B_0 the weak coupling assumption $||d_n|| = 1$ is indeed violated and for that reason the perturbative approach becomes inaccurate.

3.2.2. D-shaped dbm9 Case Finally, the non-axisymmetric stability of the D-shaped *dbm*9 equilibrium is studied. In this case a $n = 18$ primary toroidal mode is examined with multi-mode toroidal coupling of 7 toroidal normal modes. As can be observed from Fig.4, a similar outcome in comparison to the *cbm*18_*dens*6 equilibrium is drawn. However, in this case an order of magnitude lower applied field results in similar relative coupling due to stronger plasma response, which is possibly a consequence of the larger β_N. Therefore, the stronger coupling leads to a break down of the perturbative

	Growth Rate	***Balloon***	***Kink***	***Bending***
n=12				
ELITE	0.1096	-2.858E-02	-3.838E-03	2.905E-02
Reconstruct	0.1134	-2.907E-02	-3.615E-03	2.974E-02
n=15				
ELITE	0.1550	-4.325E-02	-4.648E-03	4.095E-02
Reconstruct	0.1582	-4.404E-02	-4.451E-03	4.204E-02
n=18				
ELITE	0.1876	-7.308E-02	-6.514E-03	6.536E-02
Reconstruct	0.1869	-7.448E-02	-6.298E-03	6.731E-02

Table 1: Comparison of growth rates and contributions to δW in terms of destabilising ballooning and kink/peeling terms and stabilising field line bending between the ELITE result and the reconstructed result for the *cbm*18_*dens*6 equilibrium case.

assumptions at much lower applied field strength B_N/B_0. In addition, the stronger coupling affects the variational result in the case of a triplet mode, as multiple toroidal normal modes need to be coupled for convergence to be achieved.

3.3. Variational Poloidal & Toroidal Mode Coupling

We now turn into the full variational approach, which allows the poloidal Fourier spectrum to adjust in addition to coupling of toroidal Fourier modes. Neither the perturbative method nor the "variational toroidal coupling" method discussed in Section3.2, allows changes in the coupling of the poloidal harmonics in response to the 3D MP. Since the applied field is composed of a wide range of poloidal harmonics, and strong coupling takes place at experimentally relevant applied fields, it is expected that the poloidal coupling within each toroidal normal mode will be affected. To test this hypothesis, we allow the coupling between the poloidal harmonics to change in this more general variational approach. However, in this case the axisymmetric potential and kinetic energy matrices need to be reconstructed. The reconstruction of those matrices is performed in two ways. In the first way, those matrices are input variables and taken from ELITE, provided the plasma is up-down symmetric or the low n version is not used. In the second way, those matrices are calculated considering the axisymmetric δW and δK for the displacement ELITE provides and so the low n modes or up-down asymmetric plasmas configurations can be considered.

To begin with, the circular *cbm*18_*dens*6 equilibrium is used in order to verify that the calculation of the axisymmetric and non-axiisymmetric matrices is correct. As can be observed from Table.1, where a comparison of the growth rate and the axisymmetric destabilising/stabilising energy contributions are listed, the reconstruction agrees with the ELITE result. At this stage, where the axisymmetric energies can be computed accurately, the impact of the applied field on the coupling of poloidal and toroidal harmonics can be examined.

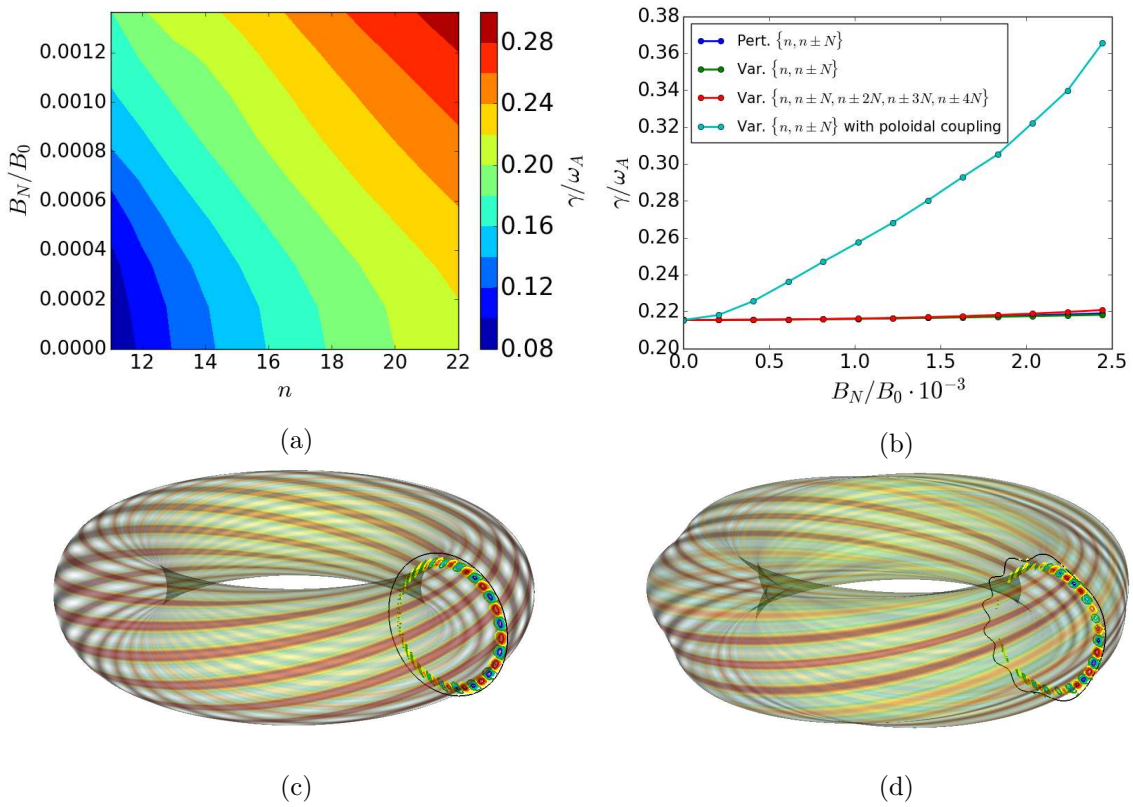

Figure 5: (a) The growth rate of the 3D triplet modes as a function of primary toroidal mode number n and applied field strength B_N/B_0 for a resonant N=3 MP. (b) Comparison between the different perturbative and variational methods for a $n = 21$ triplet mode as a function of B_N/B_0. (c) The 3D reconstruction of the structure of a $n = 12$ mode for the axisymmetric equilibrium geometry. (d) The 3D reconstruction of the structure of a triplet $n = 12$ mode for the non-axisymmetric equilibrium geometry, which is scaled by a factor of 15 such that the non-axisymmetric equilibrium displacement is visible. The black line indicates the (c) axisymmetric and (d) scaled non-axisymmetric equilibrium plasma boundary for $B_N/B_0 = 1.5 \cdot 10^{-3}$.

3.3.1. Circular cbm18 Case The circular *cbm*18*_dens*6 is considered for the even $N = 3$ MP used previously. Fig.5 illustrates the growth rate of 3D peeling-ballooning modes as a function of primary toroidal mode number n and applied field strength B_N/B_0. Initially, only first neighbour toroidal coupling is considered, i.e. triplet modes $\{n-N, n, n+N\}$, retaining all the constituent poloidal harmonics and allowing freedom in the poloidal coupling. From Fig.5a and Fig.5b it becomes apparent that the freedom in the poloidal coupling results in strong destabilisation of the ballooning mode, and for an applied field of $B_N/B_0 \sim 2 \cdot 10^{-3}$ the growth rate increased by $\sim 60\%$ in comparison to the previous methods where only a difference of $\sim 5\%$ occurred. The applied field interacts strongly with specific poloidal harmonics in such a way that field line bending is minimised and the driving terms are maximised. However, from Fig.5d it can be concluded that the resulting mode structure is in good qualitative

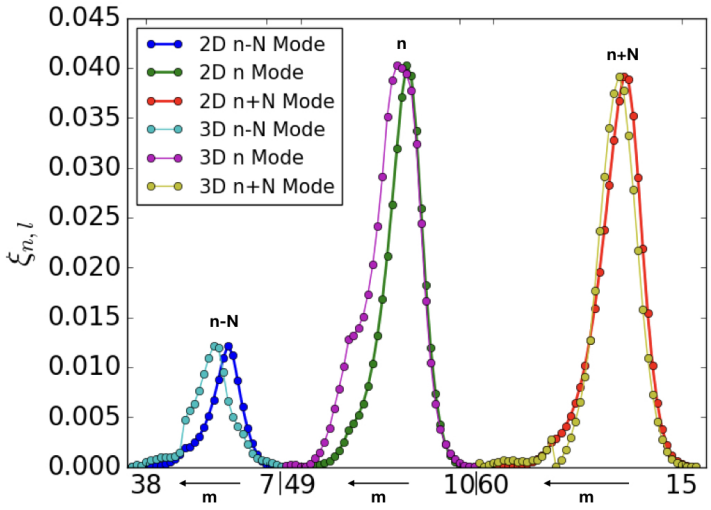

Figure 6: A comparison between the axisymmetric modes and the 3D triplet mode for the relative amplitude of the constituent poloidal harmonics for each toroidal normal mode of the $n = 12$ triplet for $N = 3$ and $B_N/B_0 = 1.5 \cdot 10^{-3}$.

agreement with the perturbative method as calculated in Ref.[27]. Direct comparison of the coupling coefficients is not possible, as the toroidal coefficients are replaced by a set of toroidal/poloidal coefficients. Nevertheless, the difference in the poloidal spectrum of the axisymmetric normal mode compared to the 3D mode can be studied. Fig.6 illustrates the relative amplitude of the poloidal coupling coefficients for each axisymmetric toroidal normal mode compared to the poloidal coupling coefficients of the 3D mode. The (independent) toroidal modes of the axisymmetric system have been normalised to the same maximum amplitude as the 3D calculation. Each toroidal mode has an increasing poloidal mode number in the left direction. As can be observed, the poloidal coupling is affected by the 3D field; in this case we find that the 3D field pushes the ballooning mode outwards in the radial direction, since the poloidal harmonics that resonate with edge of the plasma and the vacuum region are amplified. In addition, the variation with respect to poloidal coupling leads to a different relative coupling in comparison to the perturbative method since the higher sideband $n' = n + N$ is observed to be larger than the lower sideband $n' = n - N$. Within the perturbative method stabilisation would be expected for stronger coupling to the higher sideband, but the observed destabilisation in the variational approach is attributed to the difference in the poloidal coupling. Specifically, the greater coupling to vacuum modes could drive the external kink mode more.

Furthermore, the impact of MPs is examined with respect to β_N and $\Delta\phi$ variations, where $\Delta\phi$ is the phase difference between the upper and lower 3D coils that sets the parity of the applied MP field. The circular *cbm*18_*dens*6, *cbm*18_*dens*7 and *cbm*18_*dens*8 equilibria are considered for $\beta_N = [1.06, 1.31, 1.54]$ with $q_a = [2.97, 3.01, 3.04]$. Fig.7 illustrates the dependence on β_N for a $n = 15$ triplet mode

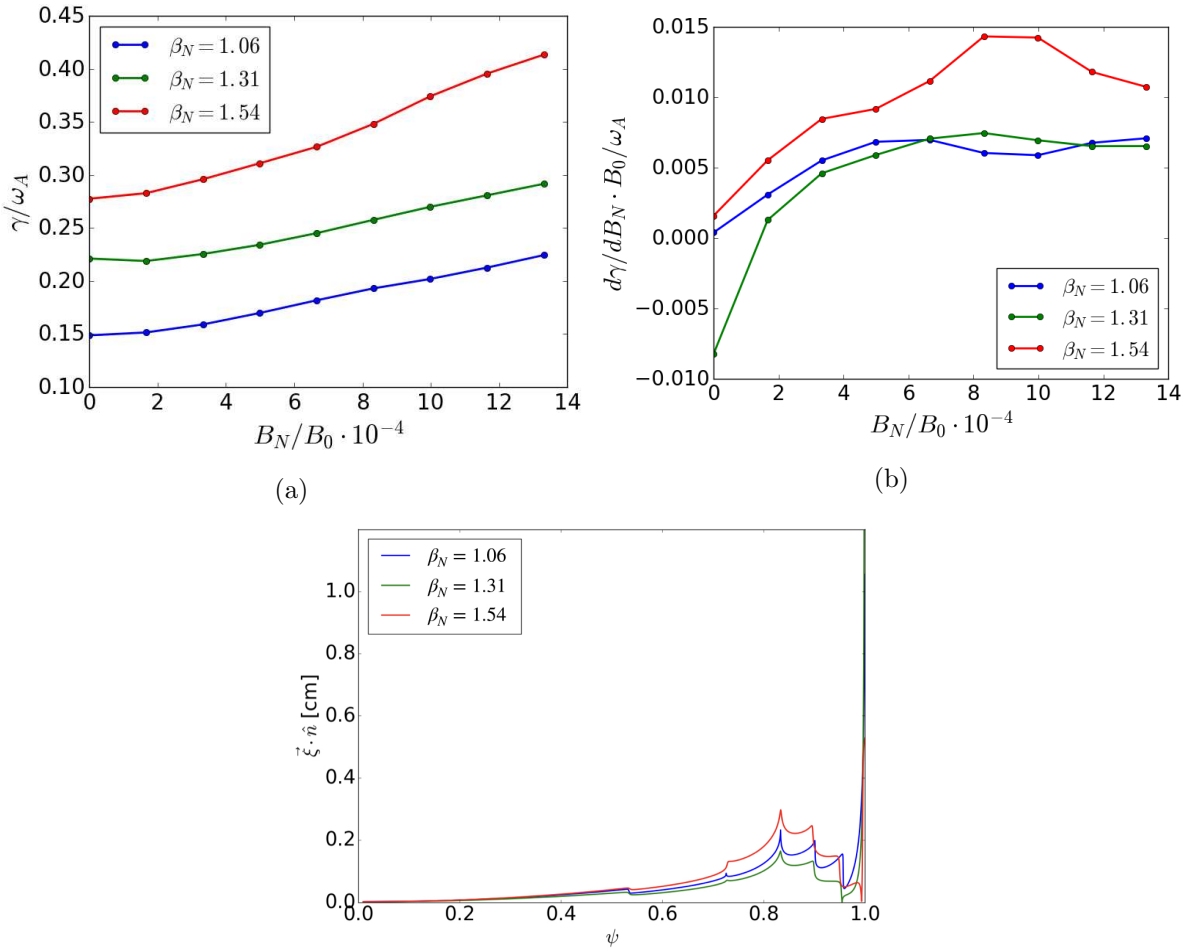

Figure 7: (a) The normalised growth rate and (b) the change in the normalised growth rate of the $n = 15$ triplet as a function of the applied field strength B_N/B_0 for different β_N for the *cbm*18 set of axisymmetric circular cross-section equilibria. (c) The non-axisymmetric equilibrium normal displacement $\boldsymbol{\delta\xi}_N \cdot \hat{\boldsymbol{n}}$ as a function of normalised ψ for applied field strength $B_N/B_0 = 10^{-4}$.

considering the even $N = 3$ MP. As can be observed, further destabilisation due to the applied MP is observed in all three cases. In addition, it can be observed that for a certain β_N the growth rate is almost linear with B_N/B_0. The stronger destabilisation occurs for the higher $\beta_N = 1.54$ case. For a fixed normal magnetic field at the plasma boundary a larger plasma response, i.e. normal flux surface displacement, is expected with increasing β_N. However, this will largely depend on the poloidal spectrum of the applied field. The maximum response within the pedestal region occurs for the $\beta_N = 1.54$ case and significant destabilisation is observed with increasing B_N/B_0. The lowest response within the pedestal is observed in the $\beta_N = 1.31$ (although the largest at the plasma boundary) and it can be observed that the fractional change in growth rate

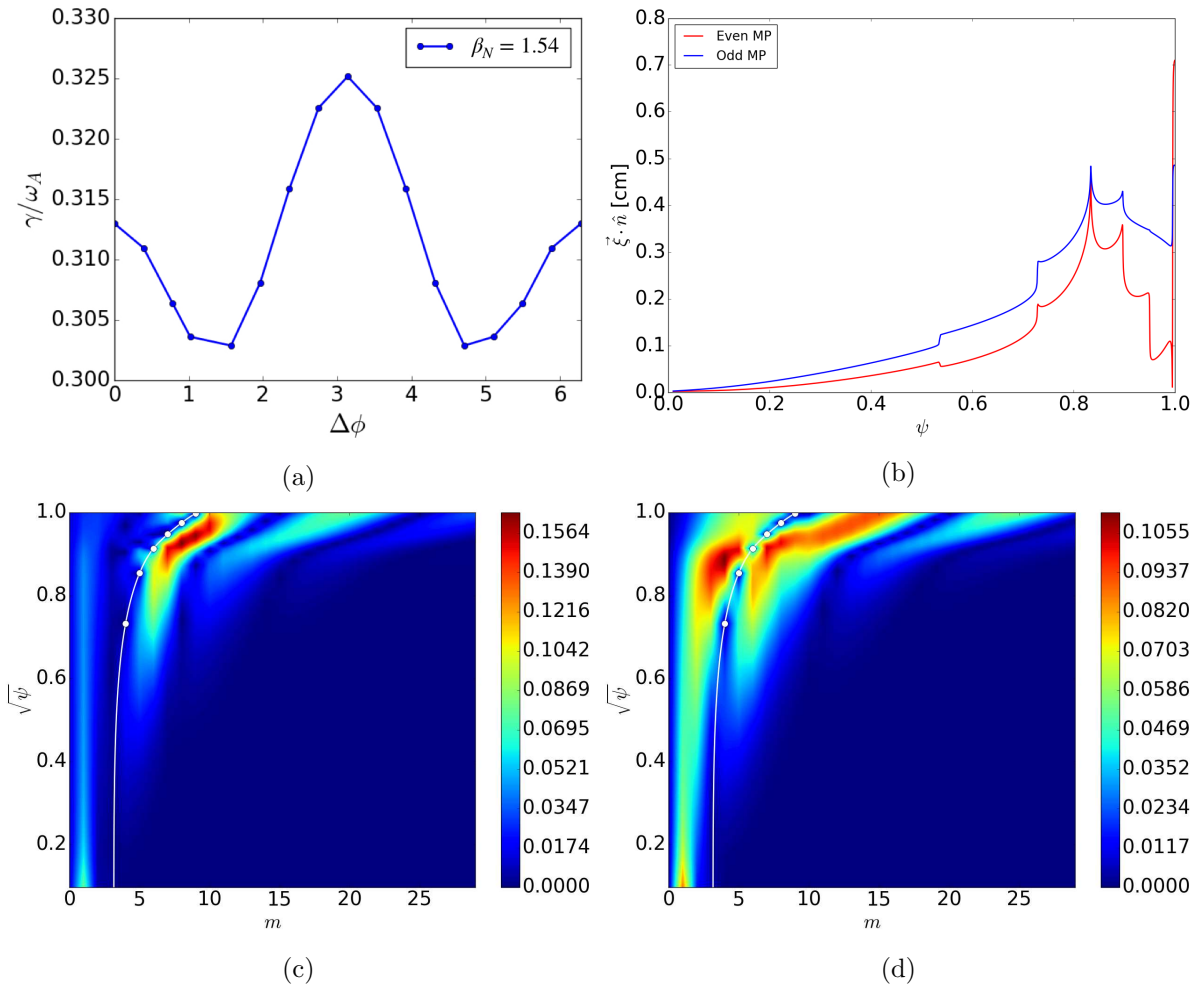

Figure 8: (a) The dependence of the growth rate of a $n = 15$ triplet on the phase $\Delta\phi$ of the imposed MP for the $\beta_N = 1.54$ *cbm*18_*dens*8 axisymmetric circular cross-section equilibrium case. (b) The non-axisymmetric equilibrium normal displacement $\boldsymbol{\xi}_N \cdot \hat{\boldsymbol{n}}$ [cm] as a function of normalised ψ for applied field strength $B_N/B_0 = 10^{-4}$. The radial dependence of the straight field-line angle mode structure of $\boldsymbol{B}_N \cdot \hat{\boldsymbol{n}}$ 10^{-4} [T] for (c) the even and (d) odd MP field.

with increasing B_N/B_0 is smaller in comparison to $\beta_N = 1.54$ and similar to $\beta_N = 1.06$. Therefore, since the relation is not linear with β_N it can be concluded that the poloidal mode structure of the applied MP itself is a crucial factor for the plasma stability.

Fig.8 illustrates the dependence of the $n = 15$ triplet for the $\beta_N = 1.54$ case on the applied MP phase, where $\Delta\phi = 0$ is the even MP and $\Delta\phi = \pi$ is the odd MP, with $B_N/B_0 = 5 \cdot 10^{-4}$. As can be observed, a small variation of the growth rate occurs with $\Delta\phi$, with the odd MP configuration resulting in the most unstable case. From Fig.8 it is clear that although the odd MP has a smaller edge displacement in comparison to the even MP indicating a less resonant response (presumably a peeling physics effect), the overall displacement in the pedestal region is larger. The additional non-axisymmetric

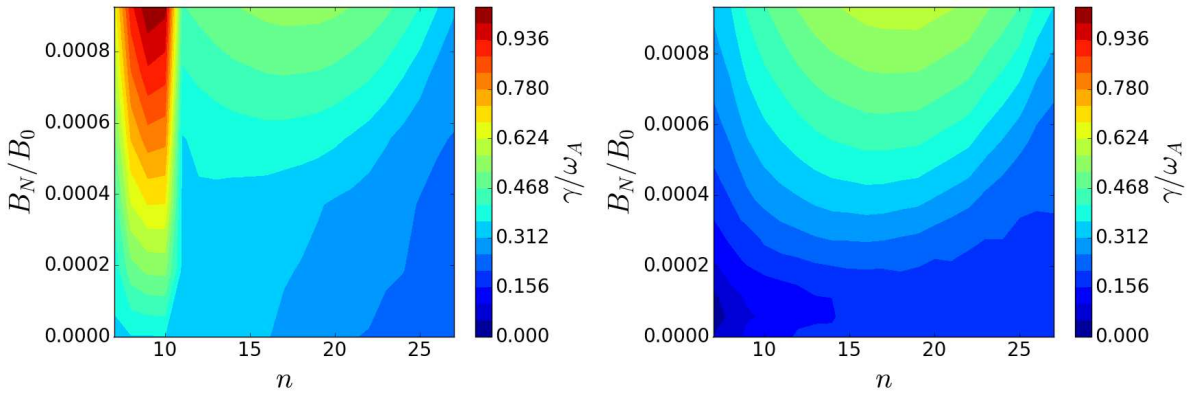

(a) (b)

Figure 9: Growth rate of the 3D triplet modes as a function of the primary toroidal mode number n and applied field strength B_N/B_0 for the *dbm*9 equilibrium case and a $N = 3$ resonant applied MP for (a) the case with no wall and (b) the case with an ideal conducting wall at $a_w/a = 2\%$.

displacement of the flux surfaces seems to further destabilise the ballooning mode, as kink/peeling modes are stable for this equilibrium. The even and odd configuration of the non-axisymmetric MP had very different poloidal spectra and this indicates once again the importance of the poloidal spectrum in the penetration of its constituent poloidal harmonics.

3.3.2. D-shaped dbm9 Case The D-shaped *dbm*9 equilibrium case has also been examined as it represents a more experimentally relevant case, and again the resonant $N = 3$ MP field is considered. Fig.9a illustrates the growth rate of the triplets as a function of primary toroidal mode number n and applied field strength B_N/B_0. For the case without an ideal conducting wall, the growth rate of triplets around the peak of the growth rate spectrum of the axisymmetric system ($n \sim 8-10$), which mainly correspond to unstable kink modes, are significantly destabilised by a factor of ~ 2.8. The rest of the triplets are also observed to be further destabilised but at lower levels and this provides an indication that kink modes become more unstable with the applied MP field. This observation is similar to the perturbative method, where strong destabilisation is expected at modes around the peak of the growth rate spectrum, due to destabilising coupling from both lower and higher sidebands. Fig.9b illustrates the growth rate when an ideal conducting wall surrounds the plasma. In this case the wall is placed close to the plasma surface $(a_w - a)/a = 2\%$ to fully minimise the kink component of the instability. As can be observed, the strong destabilisation of the kink modes is absent (as they are stable in the first place) and strong destabilisation of ballooning modes is observed especially for $n \sim 20$.

A comparison between the mode structure of the the $n = 9$ triplet in the case with and without an ideal conducting wall shows the absence of the kink instability.

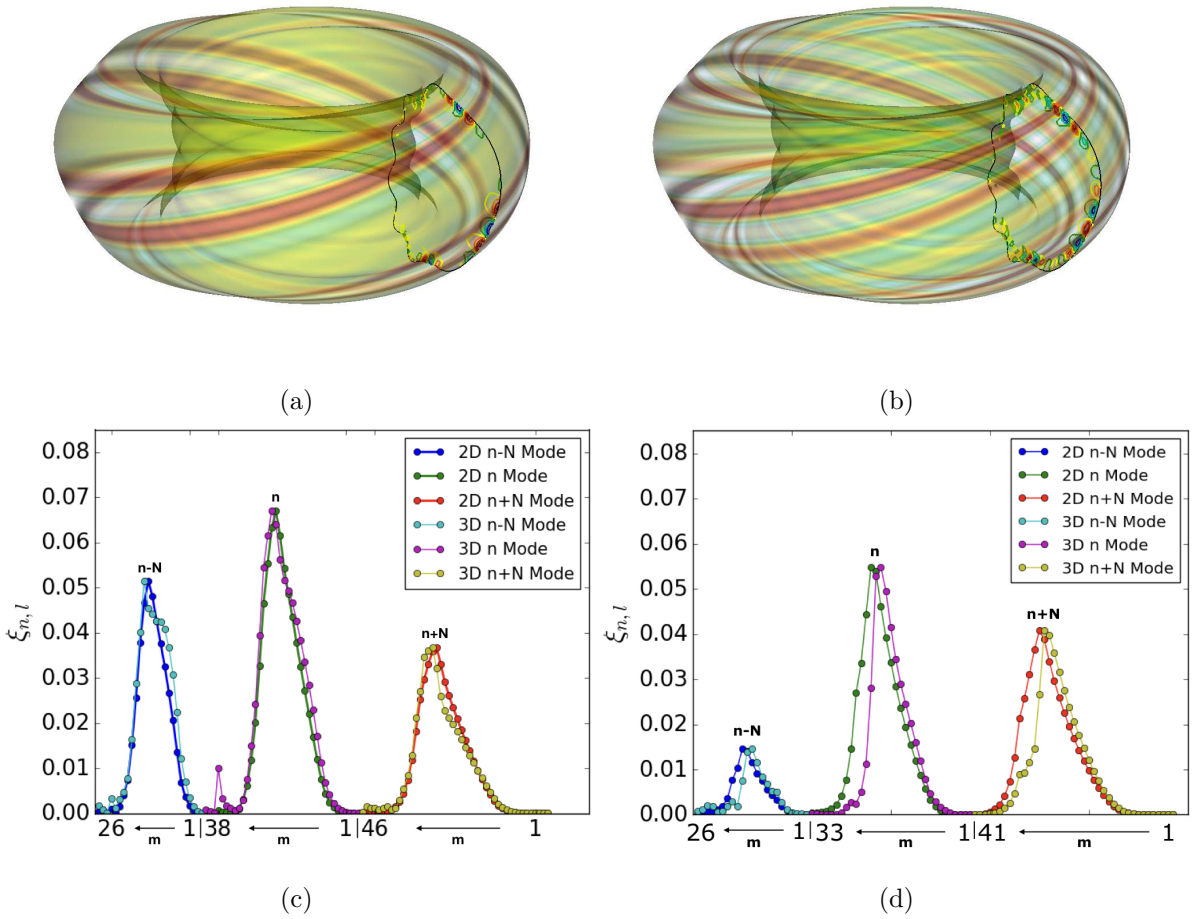

Figure 10: The 3D reconstruction of the $n = 9$ triplet mode (a) without and (b) with an ideal conducting wall. A comparison between the axisymmetric modes and the 3D triplet mode for the relative amplitude of the constituent poloidal harmonics for each toroidal normal mode (c) without and (d) with an ideal conducting wall; $B_N/B_0 = 10^{-3}$ for an even $N = 3$ MP.

Fig.10 illustrates the cases with/without an ideal conducting wall and demonstrates that the case without a wall has an external kink/peeling-ballooning structure where the displacement from the instability peaks at the very edge of the plasma surface. It can also be observed that the mode structure of the constituent toroidal harmonics is similar to their axisymmetric structure. On the other hand, the case with an ideal conducting wall has a ballooning like structure where the displacement peaks within the pedestal. In this case, it can be observed that the mode structure of the constituent toroidal modes is significantly different from their axisymmetric structure, and the mode moves radially inwards. An additional interesting feature that occurs in the case without an ideal conducting wall, is the complete reorganisation of modes away from the kink peak of the growth rate spectrum. Fig.11 illustrates the $n = 18$ triplet for

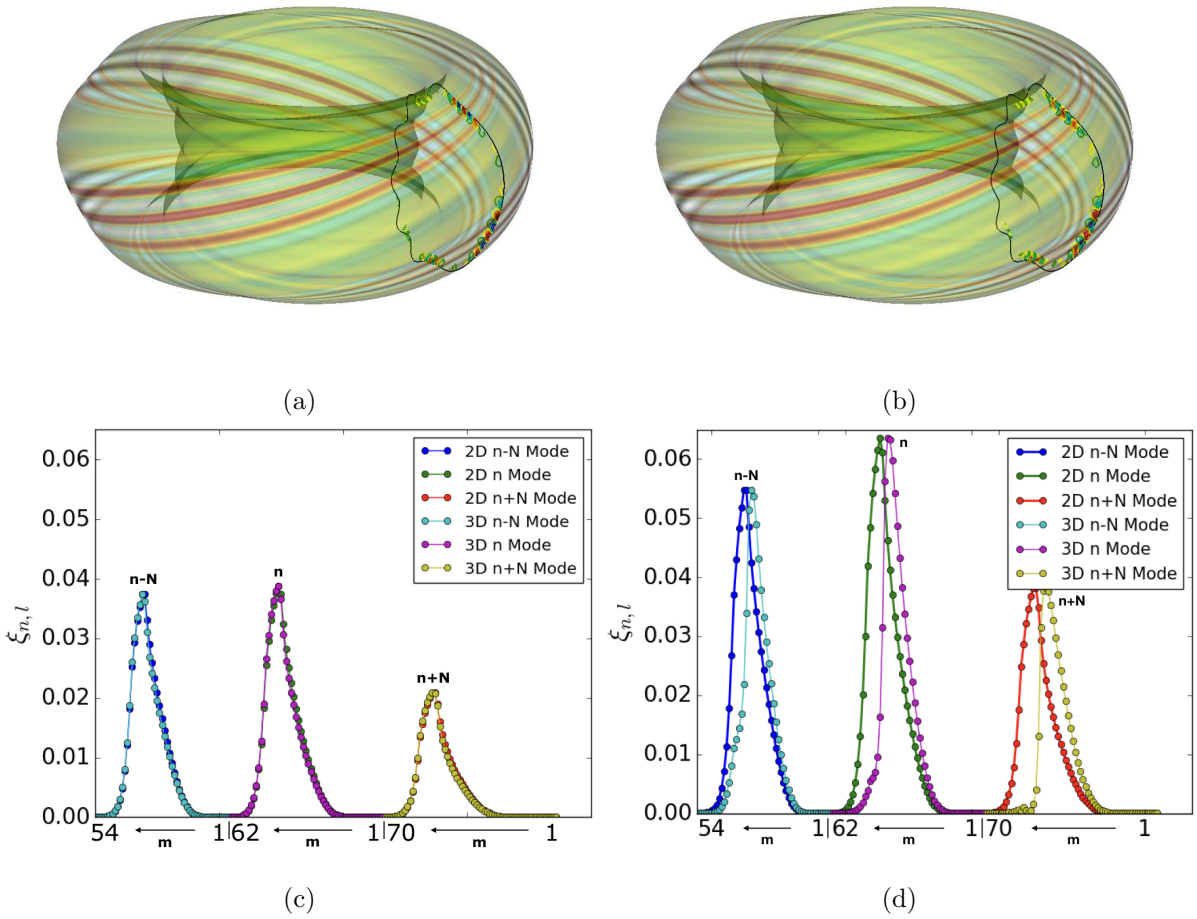

Figure 11: (a,b) The 3D reconstruction of the $n = 18$ triplet mode and (c,d) the comparison between the volume average amplitude of the axisymmetric modes and the 3D triplet mode for the constituent poloidal harmonics for each toroidal normal mode; $B_N/B_0 = 10^{-4}$ (left) and $B_N/B_0 = 10^{-3}$ (right) for an even $N = 3$ MP.

$B_N/B_0 \sim 10^{-4}$ and $B_N/B_0 \sim 10^{-3}$. The individual toroidal modes are reorganised with the external kink/peeling poloidal harmonics being minimised and the 3D mode moves radially inwards at sufficiently high $B_N/B_0 \sim 10^{-3}$. This feature is not observed for kink modes close to the peak of the growth rate spectrum $n \sim 9$, which retain their kink like structure, in the case without an ideal conducting wall (see Fig.10).

Finally, especially for the D-shaped *dbm*9 equilibrium case where strong toroidal coupling is observed even for small B_N/B_0, the impact of multi-mode coupling of the toroidal normal modes is examined, including freedom in the relative poloidal coupling. The $n = 18$ mode is considered as the primary harmonic of a triplet $\{n - N, n, n + N\}$, a quintuplet $\{n - 2N, n - N, n, n + N, n + 2N\}$ and a septuplet $\{n - 3N, n - 2N, n - N, n, n + N, n + 2N, n + 3N\}$ 3D mode for $B_N/B_0 \sim 10^{-3}$. As can be observed from Fig.12a, strong coupling occurs between the individual toroidal

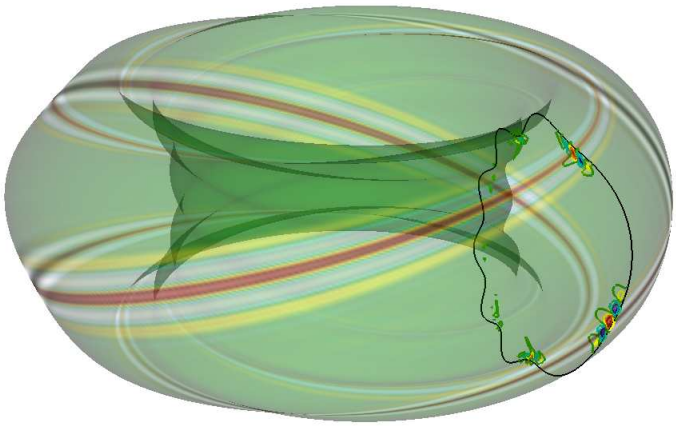

(a)

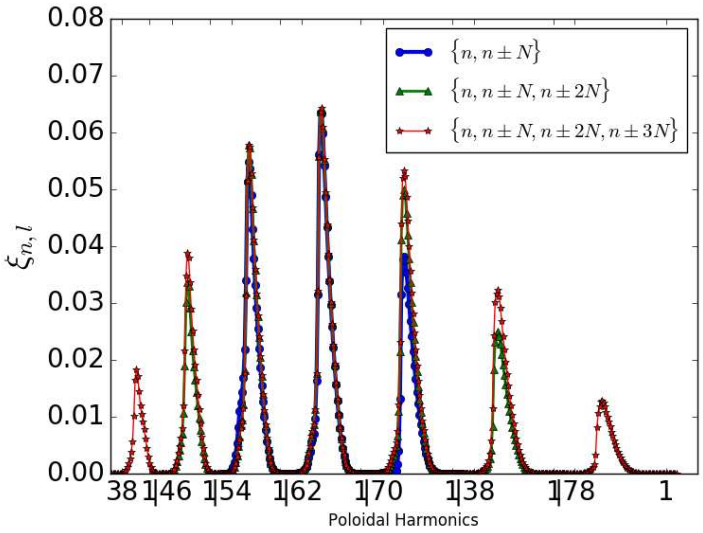

(b)

Figure 12: (a) The 3D reconstruction of the $n = 18$ septuplet mode and (b) the comparison between the volume average amplitude of the axisymmetric modes and the 3D modes for the constituent poloidal harmonics for each toroidal normal mode; $B_N/B_0 = 10^{-3}$ (right) for an even $N = 3$ MP.

normal modes even considering a septuplet mode. The relative shape of the poloidal spectrum of the individual normal modes is not significantly altered by considering more normal modes in the coupling, but their relative amplitude changes. This results in a significantly more poloidally localised 3D mode minimising field line bending, such that the growth rate of the mode increases further, from $\gamma/\omega_A = 0.55$ for the triplet to $\gamma/\omega_A = 0.62$ for the septuplet.

4. Conclusion

The linear stability of non-axisymmetric tokamak plasmas has been examined within a new numerical framework based on a variational approach that builds on the eigenvalue axisymmetric stability code ELITE. The framework first computes the linear plasma response, i.e. the new 3D equilibrium component as a result of the application of an external MP field, and the axisymmetric peeling-ballooning eigenfunctions. Considering a variational formulation of the energy principle, all this information is used to construct the linear non-axisymmetric stability of global ideal MHD modes.

The coupling of toroidal harmonics by MPs can significantly influence the ballooning instability for D-shaped high β_N plasmas, for experimentally relevant MP field strength of $B_N/B_0 \sim 10^{-5} - 10^{-3}$. This then raises questions about the use of perturbation theory to couple toroidal normal modes for realistic 3D field amplitudes. In addition, the perturbative approach does not take into account the influence of the MP field on the relative coupling in the poloidal mode structure of the triplet. In order to resolve this issue, a new more general variational approach, has been developed in this paper. This uses the individual poloidal and toroidal Fourier modes from the normal modes of the axisymmetric system, as a basis for trial functions with coefficients to be determined by minimisation of the energy functional. This is shown to provide significantly more degrees of freedom, allowing the MP field to influence the peeling-ballooning structure of each constituent toroidal Fourier mode used in the basis.

The variational method revealed the impact of the MP field in the poloidal coupling of the individual axisymmetric normal modes. The change in the poloidal coupling of the basis functions resulted in further destabilisation of ballooning modes. This is especially apparent in cases where strong toroidal coupling is observed; for example in the D-shaped *dbm*9 equilibrium case, the peeling-ballooning mode was completely reorganised and it was observed that the peeling component of the instability, i.e. poloidal harmonics that resonate in the vacuum region, were suppressed for sufficiently high applied field B_N/B_0 and toroidal mode number n. However, for kink unstable modes close to the peak of the growth rate spectrum, the external kink-like structure was retained, and those modes were highly destabilised by the 3D field. Such a feature could be relevant for experimental high β_N plasmas, where unstable internal or external kink modes are expected for low to intermediate n modes. The significant increase in the growth rate of the most unstable kink mode potentially indicates a faster ELM crash of similar mode number n; a feature which is observed experimentally in ELM mitigation [33]. In addition, since plasma shaping and wall position are important for the stabilisation of low to intermediate n kink modes, ELM suppression could be a manifestation of the absence of a strong kink peak, that results in more unstable high n ballooning modes that can be suppressed by diamagnetic effects, leading to softer transport properties and relaxation of the pedestal, i.e. no ELM crash. In any case, global plasma stability seems to be degraded by the applied MP field and could provide an insight in experimental observation that suggests unstable plasmas in regions where the axisymmetric $J_{||} - p'$

diagram indicates stable operation [20]. Therefore, differences between mitigation and suppression could be due to the competition between the stabilising relaxation of the pedestal due to density pump out and the potential degradation of the stability boundary due to the 3D effects.

Finally, due to strong coupling of toroidal modes, the notion of a triplet mode might be insufficient and more toroidal modes may be needed for an accurate representation of the 3D mode. The variational approach allows the inclusion of a whole set of toroidal normal modes. Such a case was examined retaining only toroidal coupling for the circular *cbm*18_*dens*6 equilibrium case and significant contribution from the $\pm 2N$ and $\pm 3N$ sidebands was observed leading to further destabilisation. A similar analysis was performed for the D-shaped *dbm*9 equilibrium case, but allowing freedom in the poloidal coupling of the toroidal basis functions, and a similar outcome could be drawn. The inclusion of more toroidal modes resulted in further destabilisation and stronger poloidal localisation of the peeling-ballooning mode. The strong poloidal and field-line localisation in 3D geometry is a feature that is observed experimentally in AUG in cases of ELM mitigation [18], and was successfully reproduced by theory based on a local ballooning analysis [17]. In those cases the 3D ballooning mode was localised around specific field lines, that coincided with locations where the plasma response crosses zero, i.e. $\xi_N \sim 0$. A numerical investigation in MAST using MPs, revealed similar behaviour for the 3D local ballooning mode [16]. It was shown that for those field lines, changes in local torsion lead to further destabilisation. The perturbative and variational methods for experimentally relevant B_N/B_0 provided similar results for the localisation of the mode for the circular *cbm*18 and D-shaped *dbm*9 cases. Although, the 3D mode seemed to be shifted between the region of $\xi_N \sim 0$ and $\xi_N \sim \xi_{min}$. This could indicate the contribution of the global and kink effects in the mode structure. However, due to the complex interplay of local shear/torsion, curvature and pressure gradient, a more rigorous examination is needed with respect to the non-axisymmetric energy terms in order to understand the localisation of the 3D mode. In our current formulation, it is not clear whether the different terms of the non-axisymmetric potential energy are positive (stabilising) or negative (destabilising). In general, further destabilisation is observed in all cases examined. Future work will focus on further understanding the non-axisymmetric structure and field-line localisation of the 3D global mode.

Acknowledgements

This work has been carried out within the framework of the EUROfusion Consortium and has received funding from the Euratom research and training programme 2014-2018 and 2019-2020 under grant agreement No 633053 and from the RCUK Energy Programme [grant number EP/T0122250/1] as well as the Fusion CDT Programme through the EPSRC [grant number EP/L01663X/1]. To obtain further information on the data and models underlying this paper please contact PublicationsManager@ukaea.uk. The views and opinions expressed herein do not

necessarily reflect those of the European Commission.

References

[1] ITER Physics Basis Editors *et al*, *Nuclear Fusion* **39** 2137, 1999
[2] J.W. Connor *et al*, *Physics of Plasmas* **5** 2687, 1998
[3] P.B. Snyder *et al*, *Physics of Plasmas* **9** 2037, 2002
[4] C.J. Ham *el al*, *Nature Reviews Physics* **2** 159-167, 2020
[5] R.A. Pitts *et al*, *Journal of Nuclear Materials* **438** S48-S46, 2013
[6] A. Loarte *et al*, *Nuclear Fusion* **54** 033007, 2014
[7] T.E. Evans *et al*, *Nature Physics* **2** 419-423, 2006
[8] A. Kirk *et al*, *Plasma Physics of Controlled Fusion* **55** 015006, 2013
[9] Y. Liang *et al*, *Nuclear Fusion* **53** 073036, 2013
[10] W. Suttrop *et al*, *Physical Review Letters* **106** 225004, 2011
[11] T.E. Evans *et al*, *Nuclear Fusion* **48** 024002, 2008
[12] Y.M. Jeon *et al*, *Physical Review Letters* **109** 035004, 2012
[13] Y. Sun *et al*, *Physical Review Letters* **117** 115001, 2016
[14] W. Suttrop *et al*, *Nuclear Fusion* **58** 096031, 2018
[15] M. Willensdorfer *et al*, *Physical Review Letters* **119** 085002, 2017
[16] C.J. Ham *et al*, *Physics of Plasmas* **21** 102501, 2014
[17] T.B. Cote *et al*, *Nuclear Fusion* **59** 016015, 2019
[18] M. Willensdorfer *et al*, *Plasma Physics of Controlled Fusion* **61** 014019, 2019
[19] S. Saarelma *et al*, *Plasma Physics of Controlled Fusion* **53** 085009, 2011
[20] D.A. Ryan *et al*, *Plasma Physics of Controlled Fusion* **61** 095010, 2019
[21] I.T. Chapman *et al*, *Nuclear Fusion* **52** 123006, 2012
[22] H.R. Wilson *et al Physics of Plasmas* **9** 1277, 2002
[23] A.B. Mihailovskii *et al*, *Plasma Phys. Rep.* **23** 844,1997
[24] C. Schwab, *Physics of Fluids B: Plasma Physics* **5** 3195, 1993
[25] P. Helander *et al*, *Physics of Plasmas* **20** 062504, 2013
[26] C.C. Hegna, *Physics of Plasmas* **21** 072502, 2014
[27] M.S. Anastopoulos Tzanis *et al*, *Nuclear Fusion* **59** 126028, 2019
[28] J.W. Connor *et al*, High mode number stability of an axisymmetric toroidal plasma, *Proc. R. Soc. Lond. A* 3651-17, 1979
[29] A.H. Glasser *et al*, *Physics of Fluids* **19** 567, 1976
[30] A.E.L. Lunniss, *PhD Thesis* University of York, 2016
[31] P.B. Snyder *et al*, A Practical User's Guide for ELITE, 2006
[32] M.S. Chance, *Physics of Plasmas* **4** 2161, 1997
[33] A. Kirk *et al*, *Plasma Physics of Controlled Fusion* **55** 015006, 2013